applied sciences

MDPI

Article

A Thermogravimetric Analysis of Biomass Conversion to Biochar: Experimental and Kinetic Modeling

Cătălina Călin [1], Elena-Emilia Sîrbu [1,2], Maria Tănase [3], Romuald Győrgy [4], Daniela Roxana Popovici [1,*] and Ionuț Banu [4,*]

[1] Chemistry Department, Petroleum-Gas University of Ploiesti, 39 Bucharest Blvd., 100680 Ploiesti, Romania; catalina.calin20@yahoo.com (C.C.); elena.oprescu@upg-ploiesti.ro (E.-E.S.)
[2] National Institute for Research & Development in Chemistry and Petrochemistry ICECHIM, 060021 Bucharest, Romania
[3] Mechanical Engineering Department, Petroleum-Gas University of Ploiesti, 39 Bucharest Blvd., 100680 Ploiesti, Romania; maria.tanase@upg-ploiesti.ro
[4] Department of Chemical and Biochemical Engineering, National University of Science and Technology POLITEHNICA Bucharest, 060042 Bucharest, Romania; romuald.gyorgy@upb.ro
* Correspondence: dana_p@upg-ploiesti.ro (D.R.P.); ionut.banu@upb.ro (I.B.)

Abstract: This study investigates the pyrolytic decomposition of apple and potato peel waste using thermogravimetric analysis (TGA). In addition, using Fourier transform infrared spectroscopy (FTIR), scanning electron microscopy (SEM) and energy dispersive X-ray spectroscopy (EDS), the influence of pyrolysis temperature on the physicochemical characteristics and structural properties of biochar was studied. The degradation of biomass samples was studied between 25 °C and 800 °C. Although apple and potato peel decomposition present similar thermogravimetric profiles, there are some differences that can be evidenced from DTG curves. Potato peel showed one degradation peak in the range 205–375 °C with 50% weight loss; meanwhile, the apple peel exhibited two stages: one with a maximum at around 220 °C and about 38% weight loss caused by degradation of simple carbohydrates and a second peak between 280 °C and 380 °C with a maximum at 330 °C, having a weight loss of approximately 24%, attributed to cellulose degradation. To gain more insight into the phenomena involved in biomass conversion, the kinetics of the reaction were analyzed using thermal data collected in non-isothermal conditions with a constant heating rate of 5, 10, 20, or 30 °C /min. The kinetic analysis for each decomposed biomass (apple and potato) was carried out based on single-step and multi-step type techniques by combining the Arrhenius form of the decomposition rate constant with the mass action law. The multi-step approaches provided further insight into the degradation mechanisms for the whole range of the decomposition temperatures. The effect of temperature on biomass waste structure showed that the surface morphologies and surface functional groups of both samples are influenced by the pyrolysis temperature. A higher pyrolysis temperature of 800 °C results in the disappearance of the bands characteristic of the hydroxyl, aliphatic, ether, and ester functional groups, characteristic of a porous surface with increased adsorption capacity. Therefore, this study concludes that biomass waste samples (apple and potato) can produce high yields of biochar and are a potential ecological basis for a sustainable approach. The preliminary adsorption tests show a reasonably good nitrate removal capacity for our biochar samples.

Keywords: biomass waste; biochar; kinetic analysis; proximate analysis; thermal stability

check for updates

Citation: Călin, C.; Sîrbu, E.-E.; Tănase, M.; Győrgy, R.; Popovici, D.R.; Banu, I. A Thermogravimetric Analysis of Biomass Conversion to Biochar: Experimental and Kinetic Modeling. *Appl. Sci.* **2024**, *14*, 9856. https://doi.org/10.3390/app14219856

Academic Editors: Luca Fiori and Francisco Jesús Fernández Morales

Received: 26 August 2024
Revised: 8 October 2024
Accepted: 22 October 2024
Published: 28 October 2024

Copyright: © 2024 by the authors. Licensee MDPI, Basel, Switzerland. This article is an open access article distributed under the terms and conditions of the Creative Commons Attribution (CC BY) license (https://creativecommons.org/licenses/by/4.0/).

1. Introduction

One significant source of biochar is biomass. The carbon-rich byproduct of thermally breaking down biomass is called biochar (pyrolyzed biomass) [1]. The use of biochar as a soil additive has gained a lot of interest because it improves soil carbon sequestration, which lowers atmospheric CO_2 levels [2]. In addition to sequestering carbon in the soil, biochar has the potential to act as a fertilizer and as a soil improver.

In recent years, due to its physicochemical properties, such as porosity and surface functioning, the development of carbonaceous materials, like biochar, has attracted the interest of researchers [3]. According to the kinetic and characterization results obtained by Koçer, et al. [4], it was understood that Aloe vera leaf waste is a very suitable source for biochar production and the obtained biochar can be evaluated in different fields such as adsorption, agriculture, and combustion. The experimental work presented by Kwapinski, Byrne, Kryachko, Wolfram, Adley, Leahy, Novotny, and Hayes [2] focuses on the physical properties and compositions of the produced biochar, willow (*Salix* spp.) and pine (*Pinus sylvestris*). Various fruit-waste-based biochars were used as effective materials to remove a variety of contaminants, including both organic and inorganic pollutants [5] because fruit peels have a high concentration of functional groups (such as carboxylic groups, amino, and phenolic compounds) on their surface. Previous studies [6] have demonstrated the benefits of fruit waste as an inexpensive adsorbent that is also environmentally friendly, widely available, highly efficient, and with low treatment requirements.

Approximately one-third of global food produced is estimated to be lost and these wastes have been estimated at 1 trillion USD per year. Potato is a primary edible crop, with an annual production of 370 million tons. In recent years, EU countries have significantly increased the percentage of fresh potatoes used in processing industries, even for human consumption. The top countries with industrial potato processing are the Netherlands with 67%, Denmark with 44.6%, and France with 40.8%, respectively. In 2020, Romania represented about one-third of all holdings that produced potatoes [7]. A significant portion of the potato is utilized as a fresh product, while the rest is processed and consumed as dry potato, starch, chips, and fries [8]. Processed potatoes were valued at 10 billion euros in the European Union in 2017, which is 1.5% of the total production value of the European food industry, according to EUROSTAT [9]. The most popular potato product that is processed—producing an enormous amount of potato peel as a byproduct—is potato chips. Potato peel is a zero-value byproduct, which occurs in huge amounts after processing. Depending on the peeling method used, it ranges from 15 to 40% of the first product mass [10]. Most of the waste produced by potato processing industries is either disposed of in landfills, resulting in environmental repercussions, or utilized as animal feed, with low added value in the production chain [11]. Recently, the utilization of potato processing byproducts as biomass sources for energy and biogas generation has been proposed [12].

The worldwide apple production is estimated at approximately 75 million tons. Based on the 2020 data from Eurostat [13], Romania has the third position (15.38%) in the Southeast Europe region and is among the top five apple-producing European countries. Moreover, Romania accounted for around 11.75% of total apple production and 4.54% of overall apple production among the 27 European nations [14]. Approximately 18% of global apple production is usually converted into various products, including jams, syrups, purees, and beverages. This results in a significant quantity of byproducts whose disposal may lead to environmental contamination and incur additional costs for food manufacturing plants. The byproducts generated from the apple processing facility mostly comprise pomace produced during juice extraction and peels resulting from the manufacturing of sauces, canned apples, dried rings, and purees [15]. Peels are viewed as substantial waste, while the entire fruit is utilized for consumption or processed into further items post-peeling. The peels are either utilized for feeding purposes or discarded as rubbish [16]. For example, Enniya, et al. [17] prepared and tested the biochar obtained from apple peels (ACAP) to remove chromium (VI) from an aqueous solution. The results of the research showed that ACAP has an adsorption capacity that is higher than that of commercial activated carbon and can be considered as an efficient, inexpensive, and natural adsorbent for removing chromium (VI) from contaminated wastewater. Another study [18] investigated the preparation of banana peel biochar (BPBC) using a slow pyrolysis method and its use as adsorbent to remove diesel oil from water. The results showed that BPBC exhibited high porosity, thermal stability, and a hydrophobic character, making it a promising adsorbent for oil–water separation and environmental remediation. The adsorption capacity of BPBC

for diesel oil removal was 5.3352 g diesel oil/g adsorbent. Furthermore, banana peel biochar has been shown to be an effective adsorbent for multiple pollutants, including tetracycline, benzoic and salicylic acid, cadmium, As and Pb, Cu, ciprofloxacin and acetaminophen, and bisphenol A and doxycycline [19].

The potential of orange peels as a low-cost adsorbent was examined by Zhang et al. [20] on three different pollutant aqueous solutions, methylene blue (MB), tetracycline (TC), and fluorescein sodium (NaFL). The results obtained suggested that the absorbent had excellent adsorption capacity for MB, TC, and NaFL pollutants of 10 mg L^{-1}, with adsorption rates of 99.17%, 73.5%, and 94.24%, respectively. Amin, et al. [21] investigated with good results the biochar derived from orange peels for removing Cu^{2+} and Cd^{2+} in aqueous media.

The bio-adsorbent derived from potato peels is another type of biochar that can interact with heavy metal ions present in water and adsorb them to the surface due to its functional groups. According to Ullah, et al. [22], under optimal conditions of pH 9, 60 min contact time, 0.5 g of adsorbent, and 10 mg/L of sample concentration, potato peel biochar showed an adsorption efficiency of 61% for removal of various heavy metals such as Co^{+}, Mg^{+}, Fe^{+}, Pb^{+}, and Cd^{+}. Kyzas and Deliyanni [23] prepared modified activated carbons from potato peels as green environmentally friendly adsorbents for the treatment of two drug compounds (dorzolamide and pramipexole) from synthetic aqueous effluents. The main advantage of the carbon materials was their reusability, since the biochar that was hydrothermally treated lost just 11% of its adsorption capacity in 20 cycles and the pyrolyzed-treated carbon sample around 35%. Although, as previously presented, biochar obtained from food waste has a huge potential to replace conventional adsorbents such as activated carbon, demonstrating a good large-scale potential application in wastewater remediation; the preparation process is very important because it can influence its adsorption capacity. Carbonization, pyrolysis, hydrothermal liquefaction, and gasification are processes that can be used to produce biochar from a variety of feedstock types, including woody biomass, agricultural biomass, aquatic biomass, food and kitchen wastes, and industrial and urban wastes [24]. Operating parameters such as temperature, heating rate, and reaction time must be closely monitored since they have the potential to alter the chemical and physical characteristics of biochar [25]. Therefore, biochar produced by the pyrolysis process at temperatures between 400 and 600 °C has a high fixed carbon content but a low surface area and porosity [26], meanwhile high temperature, low pressure, and high heating rate of the pyrolysis process produces biochar with higher carbon content and a large specific surface area [27]. Biomass consists of hemicelluloses, cellulose, lignin, and small amounts of extractives, which are pyrolyzed at various temperatures and heating rates. The temperature range within which specific components of biomass decompose is as follows: between 200 and 260 °C, hemicellulose broke down first, followed by cellulose (240 to 350 °C) and lignin (280 to 500 °C or higher) [3]. Consequently, a complete understanding of the chemical processes that take place at each stage of the thermochemical degradation of biomass and the influence of process parameters on the structural properties of biochar is necessary. To replicate the pyrolytic processes of biomass at the microscale, thermogravimetric analysis (TGA) is the perfect tool. The application of TGA involves studying changes in materials and products by following patterns related to changes in weight loss with respect to temperature and time [28]. Several studies have investigated biomass pyrolysis of different biomass types using thermogravimetric analysis [29–32].

A thorough grasp of a biomass feedstock's pyrolysis kinetics is crucial for process design, feasibility analysis, and scalability in industrial applications. Thermogravimetric analysis (TGA) is the most commonly used tool to obtain experimental kinetic data for lignocellulosic biomass pyrolysis [33,34]. There are two kinds of methods used for the analysis of biomass pyrolysis kinetics: model-fitting and isoconversional methods [35]. The uncertainty in estimating kinetic parameters caused by the use of model-fitting methods can be avoided by the use of isoconversional methods. Cai, et al. [36] reviewed the general TGA data processing procedure for isoconversion kinetic analysis of lignocellulosic biomass pyrolysis by using the Friedman isoconversion method.

For studying bioresource valorization, different types of mathematical techniques and optimization algorithms have been used in the published literature [37,38]. An important aspect is the kinetic investigation of biomass decomposition, the essential step that provides data on its energy potential following thermochemical processes [39,40]. Santos, Araujo, Ribeiro, Colpani, Lima, Tenório, Coleti, Falcão, Chaar, and de Souza [31] carry out such studies on peach palm seeds (Bactris gasipaes (Kunth)) from the Amazon region. The applied kinetic methods were FWO, KAS, Starink, and Vyazovkin, and the reaction mechanism was determined by the Criado method. There are also kinetic studies on the energy transformation of beech wood biomass [41] as well as Mediterranean biomass [42] using different methods for determining kinetic parameters (activation energy and pre-exponential factor) based on the Kissinger method, isoconversion methods (Kissinger–Akahira–Sunose and Friedman), and other methods based on mathematical models (nonlinear least square minimization and optimization by genetic algorithm) and distributed activation energy model [DAEM]). The KAS method was also used for determination of activation energies from Mushroom Residue Blended with Pine Sawdust/Wheat Straw [43]. Jemaa, et al. [44] used the Coats–Redfern Model to extract kinetic parameters from Tunisian local biomass thermogravimetric data and calculated the activation energy, the pre-exponential factor, and ordinal reaction factor.

To understand the details involved in the processing of biomass waste, it is imperative to not only comprehend the stages of the biomass pyrolysis process but also to understand the specifics of the reaction kinetics.

The present research is based on an extensive search of academic literature, using the Web of Science (WOS) database, and the keyword: TS (Biomass) AND (TS=(biochar)) AND TS=(pyrolysis) AND TS=(kinetic analysis) AND (TS=(TGA)) OR TS=(Thermogravimetric Analysis). After finding the relevant papers (201 documents: 195 article types, 2 proceeding papers, and 3 review articles), we performed a cluster analysis with VOSviewer version 1.6.20, as seen in Figure 1 presenting the co-occurrence keyword diagram, which visually maps the relationships between key concepts associated with biomass, biochar, pyrolysis, and kinetic analysis. In the co-occurrence analysis, we included author keywords, while setting the minimum number of keyword occurrences to 5, resulting in a map with 21 thresholds. The centrality and connectivity of keywords, such as “pyrolysis”, “biochar”, “biomass”, and “kinetic analysis”, indicate their significant role in the research landscape related to thermogravimetric analysis (TGA) and thermal decomposition processes.

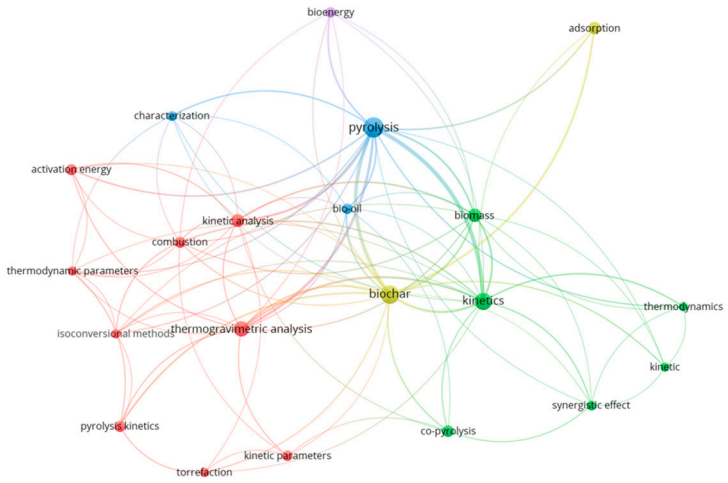

Figure 1. Co-occurrence analysis of keywords.

The figure has different clusters represented by color-coded nodes:

Red Cluster—Focuses on thermal analysis techniques like thermogravimetric analysis (TGA), kinetic parameters, and combustion; Green Cluster—Focuses on biomass conversion, thermodynamics, and biochar production, which is relevant to the investigation into

the influence of pyrolysis temperature on biochar properties; Yellow Cluster—Relates to the synergies in pyrolysis, adsorption properties, and surface characteristics of biochar; Blue Cluster—Represents characterization techniques and energy-related topics, potentially linking to the bioenergy applications of the pyrolysis process.

What distinguishes this study from the broader research field evidenced in the diagram is its specific combination of methodologies and its focused investigation into the pyrolytic behavior of apple and potato peels—biomass types that are less frequently studied in this context. The use of multiple analytical techniques (FTIR, SEM, and EDS) to study the effect of pyrolysis temperature on the structural properties and surface chemistry of biochar adds significant depth to the research. This multidisciplinary approach is not always covered in similar studies.

Hence, this study aims to investigate the impact of pyrolysis temperature on the kinetic parameters, physicochemical characteristics, and structural properties of apple and potato peels. The TGA was used to evaluate the pyrolytic decomposition of apple and potato peel waste. The kinetic analysis was performed based on single-step and multi-step models, and the results provided a thorough insight on the different mechanisms on the entire decomposition spectrum. The novelty of this research, according to our search in the Web of Science (WOS) database using terms "(biochar) AND (apple peel) OR (potato peel) AND (nitrate removal)", can be found in the investigation of both the pyrolysis behavior and the adsorption potential of biochar produced from biomass waste sources. By focusing on the detailed kinetic analysis, surface characterization, and adsorption potential of biochar from apple and potato peel, we believe this work fills an important gap in the current body of literature and adds new insights to sustainable biochar production and its environmental applications.

2. Experimental Section

2.1. Materials

Apple peel and potato peel raw material were obtained from apple and potatoes bought from local supermarkets (Ploiești, Romania).

2.1.1. Preparation of the Biomass

Apple peel and potato peel raw waste was washed with distilled water, then it was oven-dried at 50 °C for 24 h and cut into smaller portions. The obtained dried peel was finely crushed and sieved to a powder with particle sizes $\leq$ 200 μm [45].

2.1.2. Fourier Transform Infrared Spectroscopy (FTIR)

Shimadzu IRTRACER-100, Kyoto, Japan was used for conducting the FTIR analysis, in the region of 4000–400 cm^{-1} with a resolution setting of 4 cm^{-1}.

2.1.3. Thermogravimetric Analysis (TGA)

Thermogravimetric analysis utilized the thermogravimetric/derivative equipment TGA/DTG (TGA 2 Star System Mettler Toledo, Zurich, Switzerland) to evaluate the thermal stability of biomass and biochar. The method used for our study was to vary the temperature from 25 to 800 °C with heating rate (5–30 °C/min) in a controlled nitrogen atmosphere.

2.1.4. Proximate Analysis

The contents of ash, moisture, fixed carbon, and volatile matter of peel powder were measured by the method proposed by Reza et al. [46].

2.1.5. SEM Analysis

Surface morphology analysis of the samples was studied by Scanning electron microscopy (SEM) and energy dispersive X ray spectroscopy (EDS). SEM micrographs and EDS images of mapping were obtained on FIB-SEM at 30 kV, Thermo-Fisher, Brno, Czech Republic).

3. Results and Discussion

3.1. Thermal Decomposition of Biomass Waste

3.1.1. Proximate Analysis Results

The proximate analysis of apple and potato peel waste is presented in Table 1. The selection of an effective conversion procedure is significantly influenced by the moisture content of the biomass. The processing, transportation, and storage of biomass feedstock are all impacted by the moisture content. For pyrolysis, biomass with a moisture content of less than 15% is generally favored for conversion [47]. The moisture content of the two samples varies from 2.1% for potato peel to 5.48% for the apple peel and, thus, suggests their suitability for the pyrolysis process.

Table 1. Proximate analysis of biomass waste samples.

Sample	Proximate Analysis (wt%)						
	Moisture *	Volatile Content *	Fixed Carbon *	Ash *	Protein	Lipids	Carbohydrate
Apple peel	5.48	76.73	17.23	0.56	4.31 [a]	3.48 [a]	63.84 [a]
Potato peel	2.11	75.79	18.35	5.88	11 [b]	1.75 [b]	62.4 [b]

* From this study; [a] Velciov, Rivis, Popescu, Cozma, Stoin, Anghel, Rada, and Hadaruga [45]; [b] de Andrade Lima et al. [48].

The volatile content of the samples exhibited high values of 76.73% and 75.79% for apple peel and potatoes peel, respectively. This feature is desirable since it suggests that biomass waste samples can be easily broken down through pyrolytic conversion [49]. Potato peel had the highest ash content at 5.88%. The potato peel has a higher content than the apple peel, but this value is not a large one, which influences the structural characteristics of the coal in a favorable way. This characteristic is favorable because a high ash content can cause aggregation and limit heat and mass transfer, which yields low conversion and operation costs [49].

The energy contained in carbon–carbon bonds, which contributes to biochar production is mainly represented by the fixed carbon content [50]. The fixed carbon content was recorded to be in the range 17.23 to 18.35%. According to different studies [47,51] good development of the material's surface, structure, and textural qualities is dependent on the high volatile matter content and low ash content of the fixed carbon. Therefore, based on the above affirmation, the two biomass waste samples have good potential to produce high yields of biochar.

The chemical composition of the potato peel, according to de Andrade Lima, Andreou, Charalampopoulos, and Chatzifragkou [48] consists of moisture around 6.6%, protein 11%, lipids 1.75%, total carbohydrates 62.4% from which starch 20%, cellulose 32.4%, and hemicellulose 10%. Meanwhile, the mean values of moisture, minerals (ash), proteins, fats, carbohydrates, and dietary fibers (non-starch polysaccharides and lignin) determined from three batches of summer apples grown in hilly areas of Romania, according to Velciov, Rivis, Popescu, Cozma, Stoin, Anghel, Rada, and Hadaruga [45] were as follows: 5.48 $\pm$ 0.76 moisture; 3.01 $\pm$ 0.45 ash; 4.31 $\pm$ 0.48 proteins; 3.48 $\pm$ 0.40 fats; 36.39 $\pm$ 1.23 dietary fibers; and 63.84 $\pm$ 1.53 carbohydrates.

3.1.2. Thermogravimetric Profile of the Biomass Waste Samples

The thermal stability of the biomass waste was evaluated by thermogravimetric analysis. The evolution of biomass residue thermal decomposition is presented in Figure 2 in terms of TG curves and Figure 3 in terms of DTG curves, both for apple peel (A) and potato peel (B). Also, the most important peak temperatures as well as the residue amount after decomposition are given in Table 2. Even if at first sight the two biomasses have similar decomposition pathways, there are some differences that can be evidenced from DTG curves. The degradation of biomass samples was studied between 25 and 800 °C at

different heat rates (5, 10, 20, and 30 °C/min). The weight range of the samples studied was 9–11 mg.

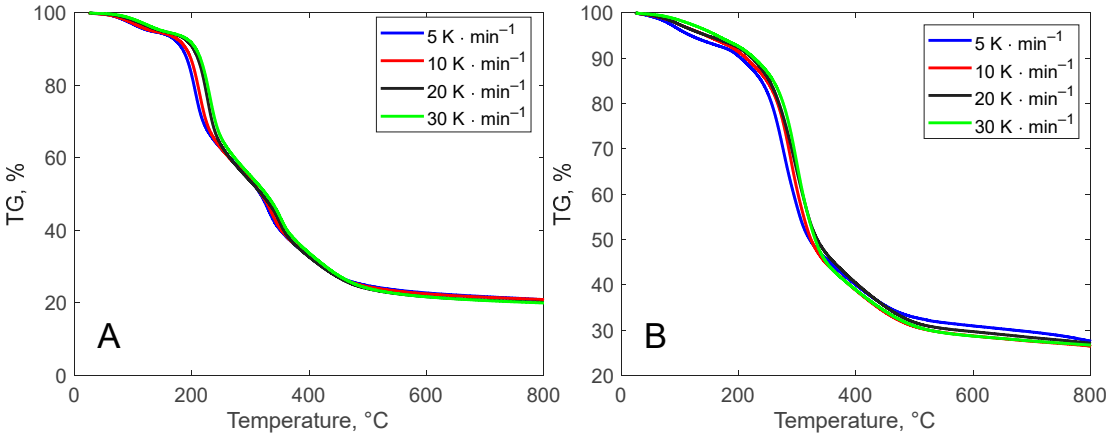

Figure 2. TG curves for apple (**A**) and potato (**B**) peel at different heating rates.

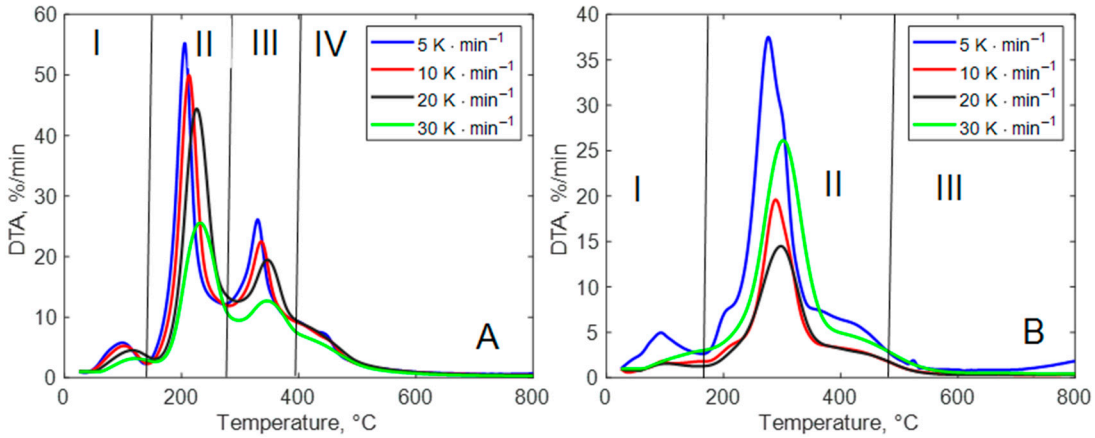

Figure 3. DTG curves for apple (**A**) and potato (**B**) peel at different heating rates (where I to IV are decomposition regions/stages referred in the paper).

Region I from these curves (Figure 3) can be ascribed to the moisture release from the biomass structure. The recorded weight loss in this region for each biomass sample is almost 5% of the initial weight. As heating rate increases, the determined weight loss values for apple peel were 5.76%/min, 5.25%/min, 4.52%/min, and 3.17%/min at 5, 10, 20, and 30 °C/min, whereas for potato peel the weight loss values were 4.95%/min, 1.81%/min, 1.51%/min, and 2.58%/min for the same heating rates.

The second stage of degradation corresponding to devolatilization differs slightly due to the composition of the analyzed sample. Apple and potato peels, which consist mostly of carbohydrates such as disaccharides and starch, exhibit distinct thermal degradation characteristics as evidenced by the DGT curves. Therefore, the potato peel showed a sharp second weight loss in the range 205–375 °C of 50%, with the maximum decomposition temperature at 297 °C, which was associated with starch pyrolysis [48]. The weight loss around 10% over 355 °C was associated with the decomposition of cellulose present in potato peel [52].

The apple peel devolatilization degradation takes place in two stages (region II and III), emphasizing that this biomass is a heterogeneous mixture, in a temperature range of 150–400 °C, similar with the one reported by Singh, et al. [53]. The first peak from 150 to 300 °C (maximum around 220 °C), with a weight loss of 38%, is caused by simple carbohydrates [45] such as fructose, glucose and sucrose [54], meanwhile, the second peak

between 280 and 380 °C with a maximum at 330 °C has a weight loss of approximately 24% attributed to non-starch polysaccharide degradation. The broad peak that starts at temperatures above 375 °C is attributed to lignin degradation [45] that occurs over a wide temperature range. These features are in accordance with literature studies [55]. The peaks that better emphasize the decomposition steps correspond to lower heating rates (5 and 10 °C/min), whereas at faster heating rates (20 and 30 °C/min), the peak shape is not well defined. The same effect can be observed for potato peel decomposition (Figure 3B).

Table 2. TG and DTA main characteristics at different heating rates.

Residue Type	Heating Rate, °C·min^{-1}	Peak Temperature, °C	$\frac{dW}{dt}$, %·min^{-1}	Residue, %
Apple peel	5	98.3 205.4 329.8	5.76 55.1 26.1	20.9
	10	101.5 212.9 335.9	5.3 49.9 22.5	20.9
	20	115.7 225.6 347.3	4.5 44.4 19.4	20.1
	30	119.9 232.1 350.0	3.17 25.6 12.7	20.0
Potato peel	5	93.6 277.9	4.9 37.5	27.5
	10	95.9 289.3	1.81 19.6	26.5
	20	93.7 297.2	1.51 14.5	27.4
	30	301.5	2.6 26.1	26.7

3.2. Thermal Decomposition Kinetic Modeling

Solid state kinetics can be investigated using thermal methods by observing changes in the sample property as it is heated or maintained at a constant temperature. In our study, reaction kinetics were analyzed using thermal data collected under non-isothermal conditions at a constant heating rate.

Through the decomposition of biomass residues, one can obtain volatile compounds (gas) and solid compounds (char); the decomposition process can be represented by the following global transformation [56]:

$$Biomass(s) \rightarrow Char(s) + Volatiles(g) \quad (1)$$

The solid samples decomposition in isothermal conditions is usually expressed as:

$$\frac{d\alpha}{dt} = k \cdot f(\alpha) \quad (2)$$

where k is the decomposition rate constant and $f(\alpha)$ is a function of conversion. The conversion or weight loss rate can be determined using the following equation:

$$\alpha = \frac{m_0 - m_t}{m_0 - m_\infty} \quad (3)$$

where m_0 is the initial weight of the sample, m_t is the weight of the sample at a certain time, and m_∞ is the final mass of the sample.

For non-isothermal TGA experiments, the heating rate (β) can be expressed in relation with time/temperature as:

$$\frac{d\alpha}{dt} = \frac{d\alpha}{dT}\left(\frac{dT}{dt}\right) = \beta\frac{d\alpha}{dT}; \quad \beta = \frac{dT}{dt} \tag{4}$$

Considering valid the Arrhenius representation of the decomposition rate constant $k(T) = k_0 \cdot e^{-\frac{E_a}{R \cdot T}}$, the conversion dependence of time in Equation (4) can be expressed as:

$$\frac{d\alpha}{dT} = \frac{k_0}{\beta}e^{-\frac{E_a}{R \cdot T}}f(\alpha) \tag{5}$$

The methods proposed in the literature for determination of the kinetic parameters from TG data are relying on Equation (5) as it is or in its integral form (differential and integral methods) [57]. Most of these methods use the graphical representation of the data for a fast visual assessment of the form of $f(\alpha)$ and the calculation of the kinetic parameters E_a and k_0. The integral form of relation (5) is defined as:

$$g(\alpha) = \int_0^\alpha \frac{d\alpha}{f(\alpha)} = \frac{k_0}{\beta}\int_{T_0}^{T} e^{-\frac{E_a}{R \cdot T}}dT \tag{6}$$

where T_0 is the initial temperature.

In relation to (2)–(6), the following variables are involved: $\frac{d\alpha}{dt}$—the rate of reaction conversion; k_0—preexponential factor $\left(s^{-1}\right)$; R—ideal gas constant (8.314 J·mol^{-1} · K^{-1}); $f(\alpha)$, $g(\alpha)$—functions characterizing the reaction mechanism; m_0, m_i, m_∞—initial, instantaneous, and final normalized mass in %; β—heating rate (°C · min^{-1}); T—temperature (K).

Different kinetic model functions $f(\alpha)$ and their corresponding $g(\alpha)$ are usually employed for the solid-state reactions, the most important among them being presented in Table 3.

Table 3. Theoretical forms of kinetic models both in differential and integral form [58,59].

Model		Differential Form— $f(\alpha)$	Integral Form— $g(\alpha)$
Power/Exponential			
Power law	P_2	$2 \cdot \alpha^{\frac{1}{2}}$	$\alpha^{\frac{1}{2}}$
	P_3	$3 \cdot \alpha^{\frac{2}{3}}$	$\alpha^{\frac{1}{3}}$
	P_4	$4 \cdot \alpha^{\frac{3}{4}}$	$\alpha^{\frac{1}{4}}$
Random nucleation and nuclei growth			
Avrami-Erofeev	A_2	$2 \cdot (1-\alpha) \cdot [-\ln(1-\alpha)]^{\frac{1}{2}}$	$[-\ln(1-\alpha)]^{\frac{1}{2}}$
	A_3	$3 \cdot (1-\alpha) \cdot [-\ln(1-\alpha)]^{\frac{2}{3}}$	$[-\ln(1-\alpha)]^{\frac{1}{3}}$
	A_4	$4 \cdot (1-\alpha) \cdot [-\ln(1-\alpha)]^{\frac{3}{4}}$	$[-\ln(1-\alpha)]^{\frac{1}{4}}$
Geometrical contraction models			
Contracting area	R_2	$2 \cdot (1-\alpha)^{\frac{1}{2}}$	$1-(1-\alpha)^{\frac{1}{2}}$
Contracting volume	R_3	$3 \cdot (1-\alpha)^{\frac{1}{3}}$	$1-(1-\alpha)^{\frac{1}{3}}$
Diffusion models			
1D diffusion	D_1	$1/(2 \cdot \alpha)$	α^2

Table 3. *Cont.*

Model		Differential Form— $f(\alpha)$	Integral Form— $g(\alpha)$
2D diffusion	D_2	$-[1/\ln(1-\alpha)]$	$[(1-\alpha)\cdot\ln(1-\alpha)]+\alpha$
3D diffusion (Jander)	D_3	$\left[3\cdot(1-\alpha)^{\frac{2}{3}}\right]/\left[2\cdot\left(1-(1-\alpha)^{\frac{1}{3}}\right)\right]$	$\left[1-(1-\alpha)^{\frac{1}{3}}\right]^2$
3D diffusion (Zhuravlev-Lesokhin-Tempelman)	D_4	$3/\left[2\cdot\left((1-\alpha)^{\frac{1}{3}}-1\right)\right]$	$1-(2/3)\cdot\alpha-(1-\alpha)^{\frac{2}{3}}$
Chemical transformation models			
Zero order	F_0	1	α
First order	F_1	$(1-\alpha)$	$-\ln(1-\alpha)$
Second order	F_2	$(1-\alpha)^2$	$[1/(1-\alpha)]-1$
Third order	F_3	$(1-\alpha)^3$	$1/2\left[(1-\alpha)^{-2}-1\right]$

3.2.1. Model-Free Methods

Different model-free methods were proposed in the published literature by Friedman [60] (Friedman method), Ozawa [61] and Flynn and Wall [62] (Flynn—Wall—Ozawa/FWO method) and Kissinger [63] (Kissinger–Akahira–Sunose/KAS method), Starink methods [64] as well as Vyazovkin method [65,66]. These are based on an isoconversional approach, with the conversion assumed to be constant and the degradation rate constant only depending on the temperature.

The KAS method is a commonly used approach for calculating the kinetic parameters. The general equation of the KAS method is [56]:

$$\ln\left(\frac{\beta}{T_m^2}\right) = -\frac{E}{R}\left(\frac{1}{T_m}\right) - \ln\left[\left(\frac{E}{A\cdot R}\right)\int_0^{\alpha}\frac{d\alpha}{f(\alpha)}\right] \quad (7)$$

where T_m is the temperature at maximum decomposition rate. By plotting $\ln\left(\frac{\beta}{T_m^2}\right)$ with respect to $\frac{1}{T_m}$ and evaluation of the slope, one can calculate the apparent activation energy.

According to the Starink method, the expressions proposed by FWO and KAS approaches can be transformed into a general equation, having the form (8) [67] that is an order of magnitude more accurate than the other two isoconversional methods (FWO and KAS).

$$\ln\left(\frac{\beta}{T^{1.92}}\right) = const - 1.0008\left(\frac{E_\alpha}{R\cdot T_\alpha}\right) \quad (8)$$

One of the most used isoconversional methods is the one proposed by Friedman, in which by taking the natural logarithm on both sides of relation (5), one can obtain [58]:

$$\ln\left(\frac{d\alpha}{dt}\right)_\alpha = \ln\left[\beta\left(\frac{d\alpha}{dT}\right)_\alpha\right] = \ln((k_0)_\alpha f(\alpha)) - \frac{E_\alpha}{R\cdot T} \quad (9)$$

In this approach, the conversion function $f(\alpha)$ is considered independent of temperature, and the degradation process depends only on the mass loss rate. The evaluation of the activation energy can be carried out by plotting $\ln\left(\frac{d\alpha}{dt}\right)$ with respect to $\frac{1}{T}$ (usually a straight line) and determining the slope of this line.

3.2.2. Model-Fit Methods

One of the most used methods for characterizing thermal decomposition kinetics is Coats–Redfren. This integral method, incorporating the degradation mechanism in its formulation, relies on Equation (10) [59]:

$$\ln\left(\frac{g(\alpha)}{T^2}\right) = \ln\left(\frac{A \cdot R}{\beta \cdot E_\alpha}\right) - \frac{E_\alpha}{R \cdot T} \quad (10)$$

From the linear plot obtained by representing $\ln\left(\frac{g(\alpha)}{T^2}\right)$ with respect to $\frac{1}{T}$, one can evaluate kinetic parameters (E_α and k_0). The discrimination among the evaluated models can be carried out based on the values of the correlation coefficient (R^2).

Kinetic Analysis

The kinetic analysis was performed by combining the decomposition rate constant Arrhenius form with the law of mass action, to evaluate the kinetic parameters for each of the decomposed biomass, considering the TG data acquired at the four heating rates taken into account. To evaluate the apparent activation energies, model-free methods were used. The linear representation of the Starink plots for the two biomass residues are given in Figure 4.

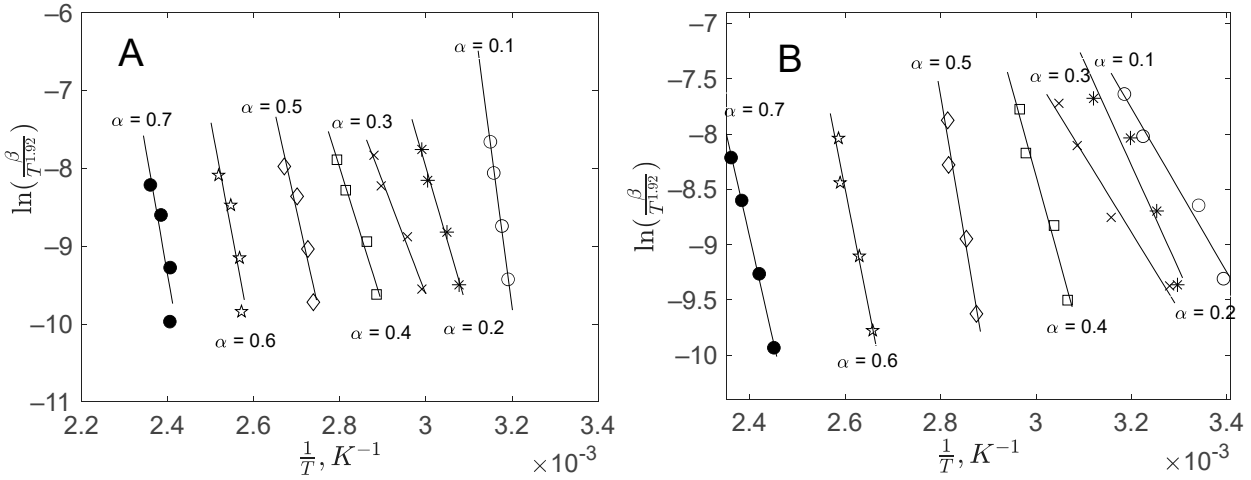

Figure 4. Isoconversional Starink plots for apple peel (**A**) and potato peel (**B**) thermal decomposition.

Single-Step Kinetic Model

Usually, when the biomass decomposition is supposed to follow a single global reaction scheme, a single-step kinetic model can be used to describe the decomposition of biomass residues. Given our results, the conversion regime for the Starink single-step kinetic model was chosen in the conversion range 0.1–0.7 both for apple and potato peel. The values of R^2 coefficients as well as slopes and intercepts for all linear regressions are given in Table 4. The apparent activation energies E_α are plotted with respect to the conversion (α) in Figure 5. The average value of E_α for apple peel was about 200 kJ · mol^{-1} and as for potato peel 130 kJ · mol^{-1}. Given that the first value of activation energy is higher, this could be due to the complexity of the biomass structure and the way different bonds are arranged in their structure. Also, it may contain some minerals that lead to an increase in the activation energy [58]. Values of the same magnitude for the apparent activation energies have been obtained in other studies published in the literature [68,69] for different bioresources' decomposition.

Table 4. Starink method results.

α	Apple Peel			Potato Peel		
	Slope	Intercept	R^2	Slope	Intercept	R^2
0.1	-4.17×10^4	123.54	0.996	-7.42×10^3	15.98	0.972
0.2	-1.90×10^4	48.91	0.987	-9.49×10^3	22.08	0.934
0.3	-1.44×10^4	33.59	0.981	-7.03×10^3	13.61	0.973
0.4	-1.76×10^4	41.42	0.975	-1.57×10^4	38.59	0.972
0.5	-2.49×10^4	58.60	0.925	-2.56×10^4	63.94	0.957
0.6	-2.94×10^4	66.10	0.848	-2.19×10^4	48.52	0.968
0.7	-3.18×10^4	67.00	0.800	-1.91×10^4	36.85	0.997

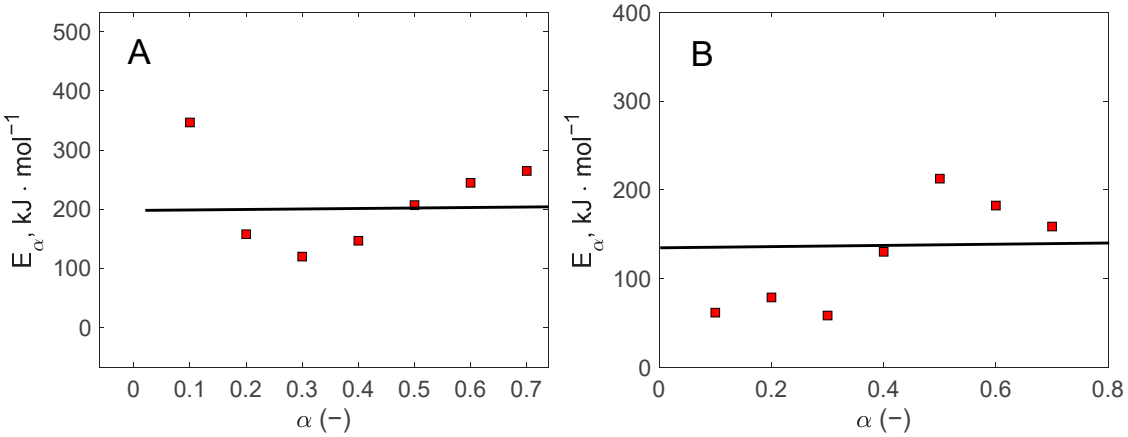

Figure 5. Apparent activation energies for different conversion values (apple peel—(**A**); potato peel—(**B**)).

Multistep Kinetic Model

In order to identify the decomposition mechanism on each region evidenced in Figure 3, corresponding to the conversion ranges given in Table 5, Coats–Redfren analysis was carried out considering the theoretical forms of $g(\alpha)$ given in Table 3. The left-hand side of Equation (10) was plotted with respect to $\frac{1}{T}$, and the adequacy of degradation mechanism was emphasized based on the R^2 coefficient in each region. For the apple peel thermal decomposition, the degradation mechanism for Stage I for conversion values below 0.1 shows 3D diffusion. This diffusion mechanism is expected, because it is associated with the presence of low volatile compounds in the structure of the bioresidues [70]. For Stage II, taking place for conversion in the range 0.1 to 0.6, the decomposition mechanism corresponds to the theoretical Avrami–Erofeev (A_4) model, which is a nucleation model where the nuclei growth describes the biomass degradation process, for which, according to the study of Emiola-Sadiq, Zhang, and Dalai [58] there is some limitation to the nuclei growth. For Stages III and IV, at conversion values above 0.6 the mechanism corresponds to third-order reaction F_3, probable to the internal rearrangement of chemical structure rich in carbon [71].

The validation of the models proposed for each stage can be carried out based on the correlation coefficients in Table 4 as well as by the parity diagrams given in Figure 6 for apple peel decomposition and Figure 7 for potato peel decomposition stages.

Table 5. Coats–Redfren analysis results.

Apple peel Kinetic parameters			
Stage I	Stage II	Stage III	Stage IV
$\alpha < 0.1$ $E_a = 6.05 \cdot 10^4 \frac{\text{J}}{\text{mol}}$ $k_0 = 2.42 \cdot 10^4\ \text{s}^{-1}$ $R^2 = 0.995$	$0.1 < \alpha < 0.6$ $E_a = 1.25 \cdot 10^4 \frac{\text{J}}{\text{mol}}$ $k_0 = 1.82\ \text{s}^{-1}$ $R^2 = 0.995$	$0.6 < \alpha < 0.8$ $E_a = 6.82 \cdot 10^4 \frac{\text{J}}{\text{mol}}$ $k_0 = 1.36 \cdot 10^6 \text{s}^{-1}$ $R^2 = 0.995$	$0.8 < \alpha < 0.1$ $E_a = 8.62 \cdot 10^4 \frac{\text{J}}{\text{mol}}$ $k_0 = 1.36 \cdot 10^6 \text{s}^{-1}$ $R^2 = 0.997$
$f(\alpha) = D_3$—3D diffusion (Jander)	$f(\alpha) = A_4$—Avrami Erofeev	$f(\alpha) = F_3$—Third order	$f(\alpha) = F_3$—Third order
Potato peel Kinetic parameters			
Stage I	Stage II	Stage III	
$\alpha < 0.1$ $E_a = 5.42 \cdot 10^4 \frac{\text{J}}{\text{mol}}$ $k_0 = 6.29 \cdot 10^3\ \text{s}^{-1}$ $R^2 = 0.991$	$0.1 < \alpha < 0.8$ $E_a = 5.13 \cdot 10^4 \frac{\text{J}}{\text{mol}}$ $k_0 = 1.62 \cdot 10^4\ \text{s}^{-1}$ $R^2 = 0.961$	$0.8 < \alpha < 1$ $E_a = 6.31 \cdot 10^4 \frac{\text{J}}{\text{mol}}$ $k_0 = 2.98 \cdot 10^6\ \text{s}^{-1}$ $R^2 = 0.988$	
$f(\alpha) = D_3$—3D diffusion (Jander)	$f(\alpha) = F_2$—Second order	$f(\alpha) = F_3$—Third order	

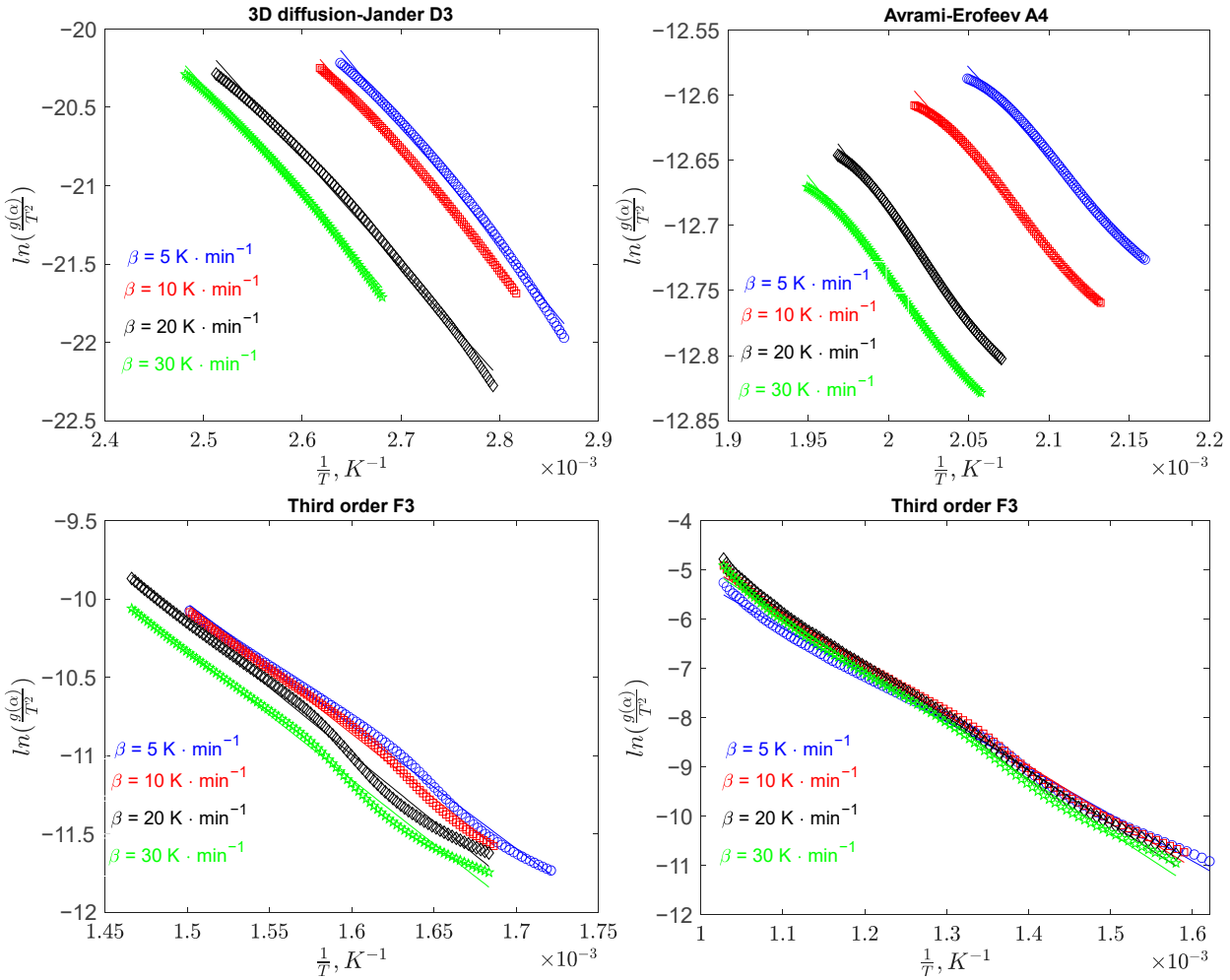

Figure 6. Coats–Redfren parity diagrams for apple peel thermal degradation.

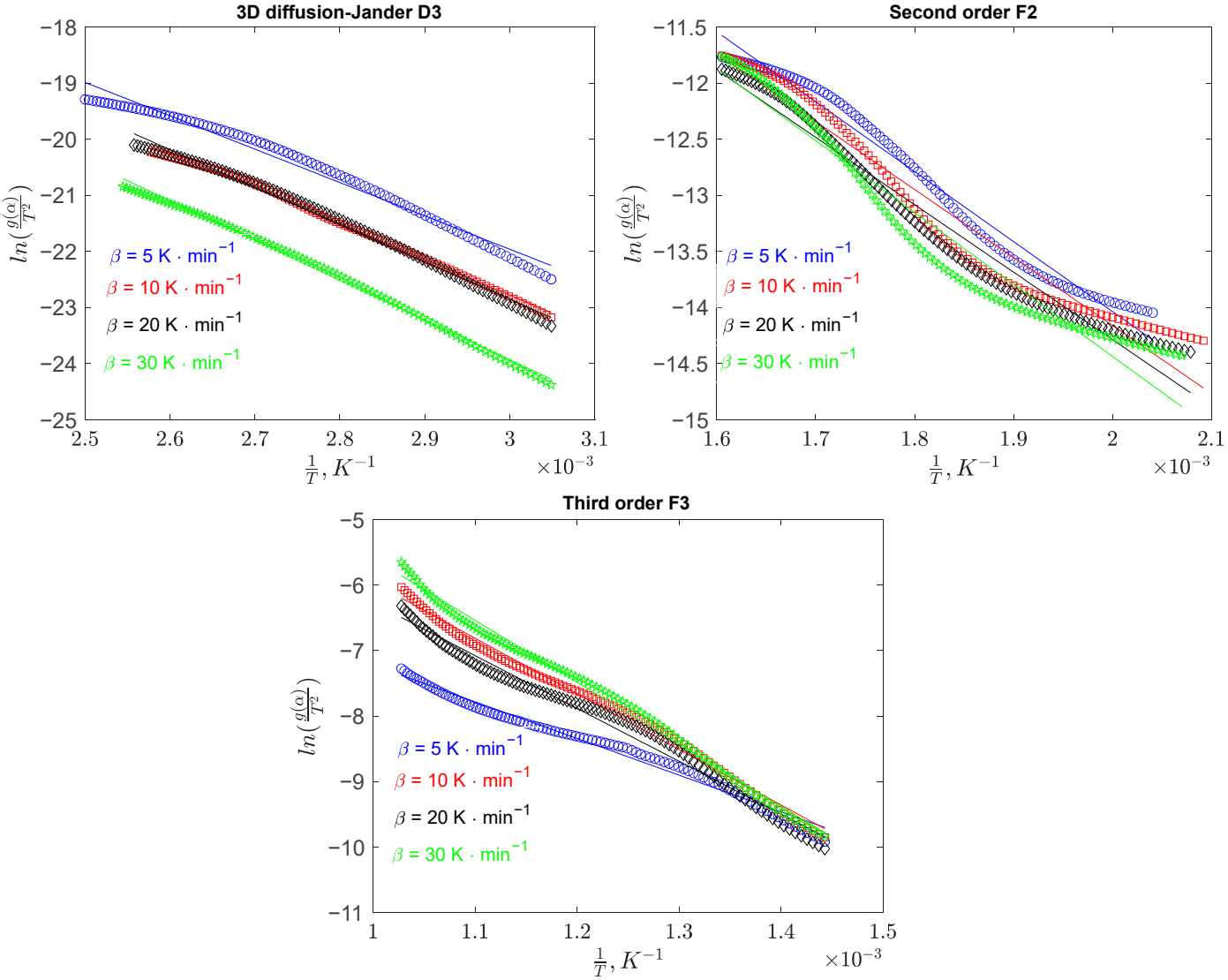

Figure 7. Coats–Redfren parity diagrams for potato peel thermal degradation.

3.3. Effect of Temperature on Biomass Waste Surface Structure

3.3.1. FTIR Analysis

Analysis of the FTIR spectra of food waste biomass, biochar, and active coal samples has demonstrated the presence of vibrations from certain specific groups such as hydroxyl, aliphatics, carboxyl and carbonyl, ester and ether, aromatic, etc. The representative peak of the hydroxyl zone is around 3300 cm^{-1}, which indicates the existence of water, carboxylic acids, phenolics, and alcohols. The intensity of these signals decreases with increasing temperature, as can be seen in Figure 8 [72]. As can be seen in Figure 8, the peak around 3233 cm^{-1} is considerably reduced for the potato-250 and apple-250 samples. The bands assigned to stretching modes of C–H groups were observed in the range of approximately 3100–2800 cm^{-1} of the FTIR spectrum, and the peak at 1373 cm^{-1} was ascribed to C−H groups, indicating the presence of methylene and methyl groups from hemicellulose and cellulose. The peak at a wavenumber of 1730 cm^{-1} was ascribed to C=O groups, signifying the existence of ketones from hemicellulose [73]. In the area of aliphatic bonds, it can be observed that they are preserved even at 250 °C but disappear at 800 °C. The absorption peak observed at 1040 cm^{-1} corresponds to the C–O stretching vibration mode (symmetric and asymmetric). This specific peak also indicates some carbohydrate functional groups (C-OH and C-OR groups) [74]. Also, the peak at 1242 cm^{-1} corresponds to the C-O bond from ester or ether, while the one at 820 cm^{-1} corresponds to C-H from aromatics [47].

Components such as the C-O bond from ester or ether (i.e., 1247, 1240, 1246, and 1242 cm^{-1}) lost their strength in the samples produced at high temperatures (800 °C). The band at 1610 cm^{-1} indicates the occurrence of C=C vibrations of the aromatic skeleton [75]. The presence of intense stretching vibrations of the C–O bonds, C=O groups, C=C, C–H, O–H, in the case of the raw material as well as the one at 250 °C may suggest their use as sorbent materials for organic and inorganic compounds [76].

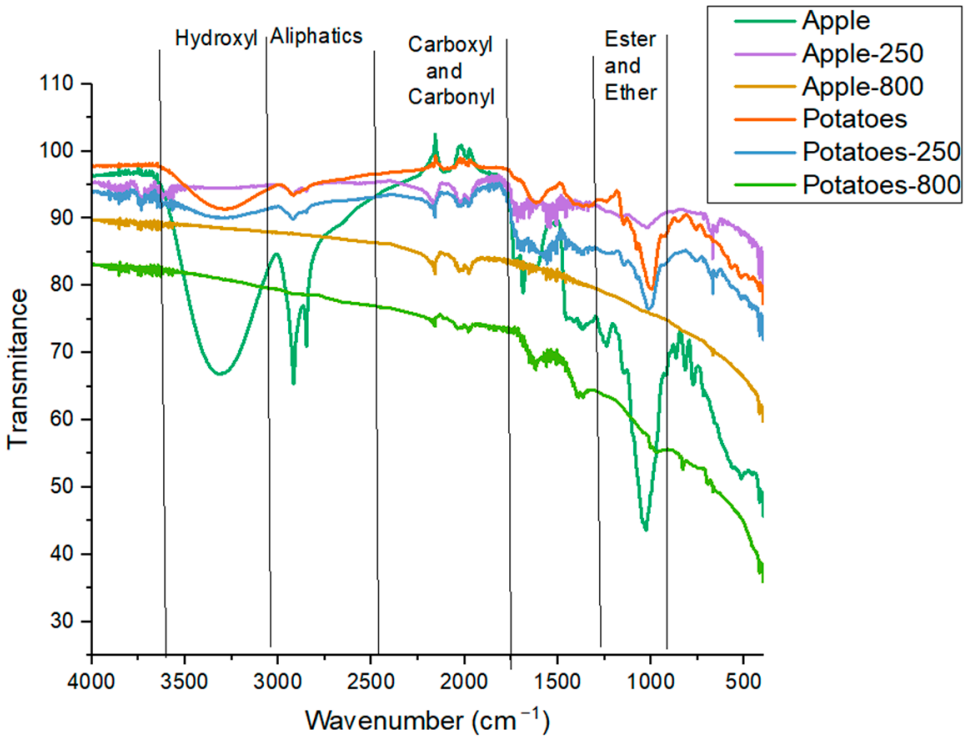

Figure 8. FTIR curves of food waste biomass and biochar.

3.3.2. SEM Analysis Results

The surface morphologies of both samples are influenced by the pyrolysis temperature, as depicted in Figure 9. When the apple and potato peels were heated to 250 °C, the resulting image displayed a smooth surface with minimal visible pores. At a temperature of 800 °C, the biochar exhibited the formation of deep porous channels, which were a result of the significant elimination of volatile organic material during the pyrolysis process. Park et al. [77] suggest that higher pyrolysis temperatures can lead to the destruction of aliphatic alkyl and ester groups and of the aromatic lignin. These observations are in correlation with the FTIR analysis, which indicates the disappearance of the bands characteristic of hydroxyl, aliphatic, ether, and ester functional groups. The elemental analysis conducted by the Energy Dispersive Spectrometer (EDS) shows that potato peel biochar pyrolyzed at 800 °C and has 66.52% carbon and 29.60% oxygen, while apple peel biochar consists of 77.78% carbon and 16.35% oxygen (Figure 10). In comparison to the ultimate analysis of potato peel, which indicates a carbon content of 43.9% and oxygen content of 46.8%, and apple waste [78,79], which exhibits a chemical composition ranging from 46.8% to 47.1% carbon and 43.6% to 46% oxygen, the reduced oxygen content in biochar confirms the loss of functional groups caused by dehydration and deoxygenation reactions during thermal treatment. This process may result in an increase in surface area and consequently enhance the adsorption capacity of the material, as stated by Streit et al. [80] and Rasool et al. [81]. The cavity's diameter measured less than 40 µm for the potato peel and less than 30 µm for the apple peel.

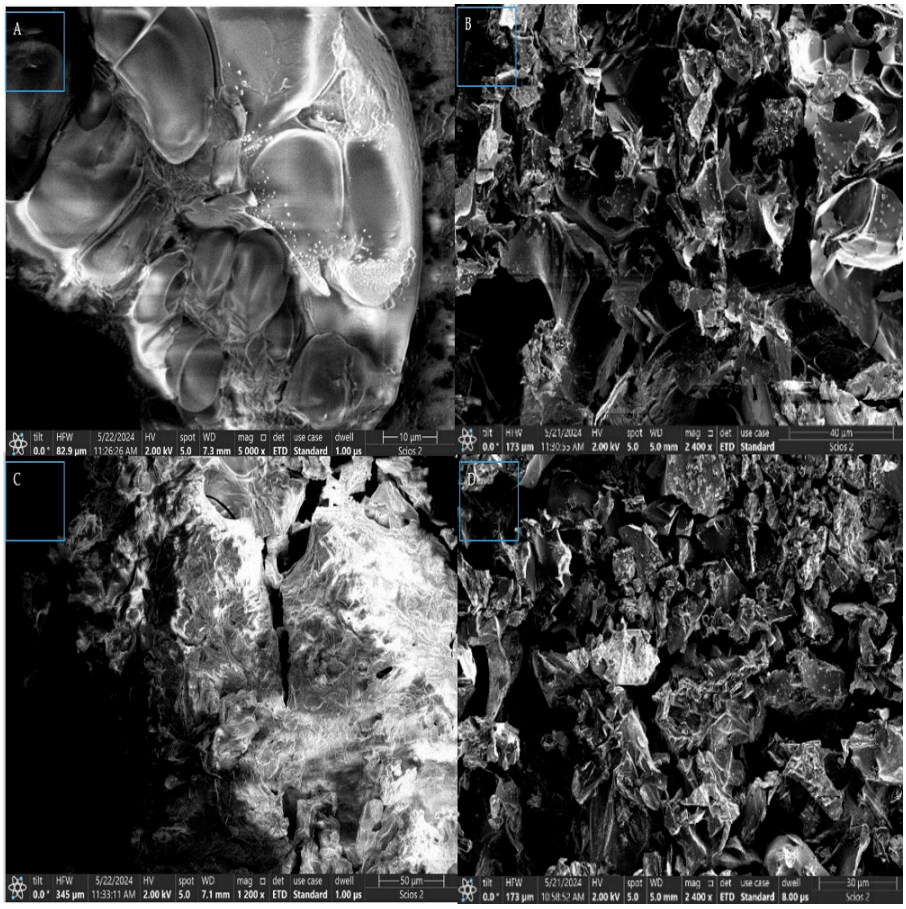

Figure 9. SEM images of (**A**) apple peel pyrolyzed at 250 °C; (**B**) apple peel pyrolyzed at 800 °C; (**C**) potato peel pyrolyzed at 250 °C; (**D**) potato peel pyrolyzed at 800 °C.

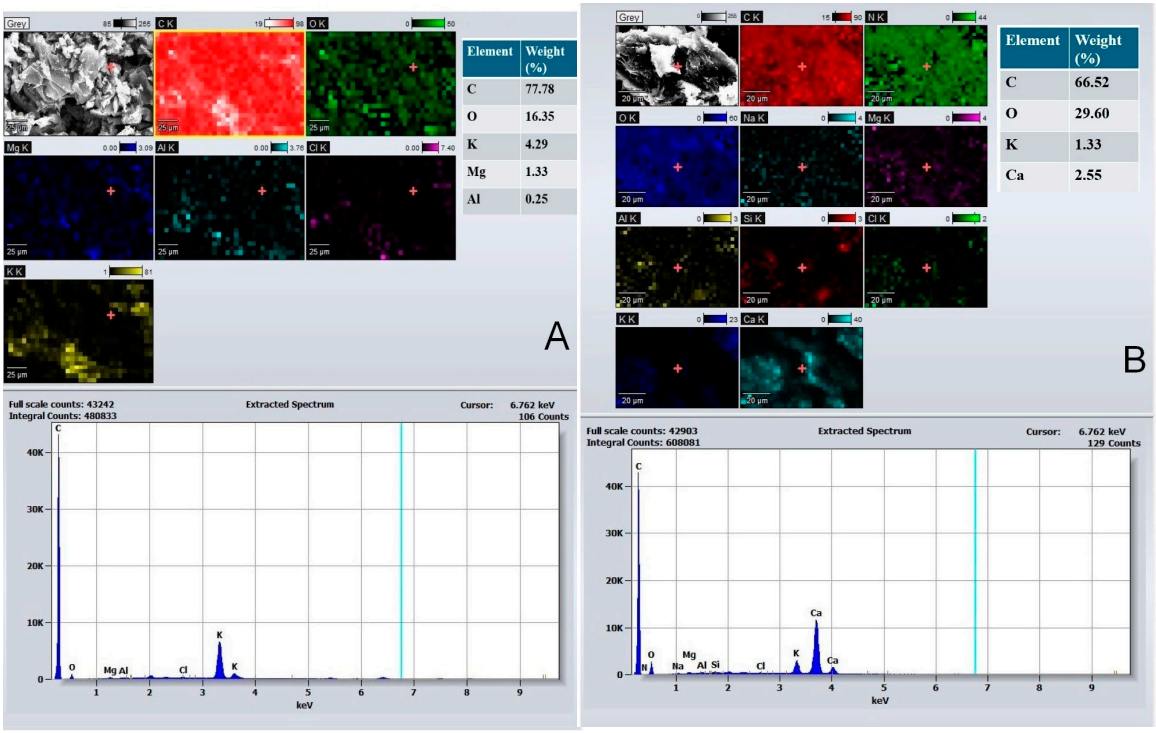

Figure 10. EDS images of (**A**) apple peel pyrolyzed at 250 °C; (**B**) apple peel pyrolyzed at 800 °C (the + sign in the figures is the cursor position where the sample was analyzed).

A preliminary study regarding the possible uses of the obtained biochars

Biochar has been tested as an adsorbent in numerous studies to remove NH_4^+, NO_3^-, and PO_4^{3-} from water either separately or in mixtures [82,83]. According to these reports, the types and characteristics of biochar as well as the environmental conditions of the aqueous phase affect the removal efficiency [84]. The surface morphology (porosity, surface area, etc.) and surface chemistry (functional group existence) of the biochar are influenced by the pyrolysis temperature, which influence the biochar's sorption capacity [85]. The feedstock characteristics also have an impact on NO^{3-} adsorption potentials [86], so more research is needed to better understand how feedstock characteristics determine NO^{3-} adsorption potentials. Our search in the Web of Science (WOS) database using terms "(biochar) AND (apple peel) OR (potato peel) AND (nitrate removal)" yielded no documents, indicating that this combination has not yet been explored. A broader search for biochar produced from apple or potato peel resulted in only 52 documents, consisting of 44 research papers and 8 review papers. Using VOSviewer software, the co-occurrence analysis was performed again, including author keywords, setting the minimum number of keyword occurrences to 5, resulting in a map with 14 thresholds (Figure 11). The density visualization map highlights the research landscape surrounding biochar, with "biochar" positioned as the central, most densely colored node, indicating that it is the primary focus and most studied area. This cluster reflects strong interest and connectivity with other related topics. Surrounding nodes like "adsorption", "removal", "pyrolysis", "biomass", and "waste" exhibit moderate density, suggesting these are also significant topics within biochar research but not central. In contrast, terms like "potato peel", "waste", and "kinetics" appear with lower density, indicating limited research in these specific areas. This visualization emphasizes research gaps, particularly in the study of biochar derived from specific agro-wastes like apple and potato peels.

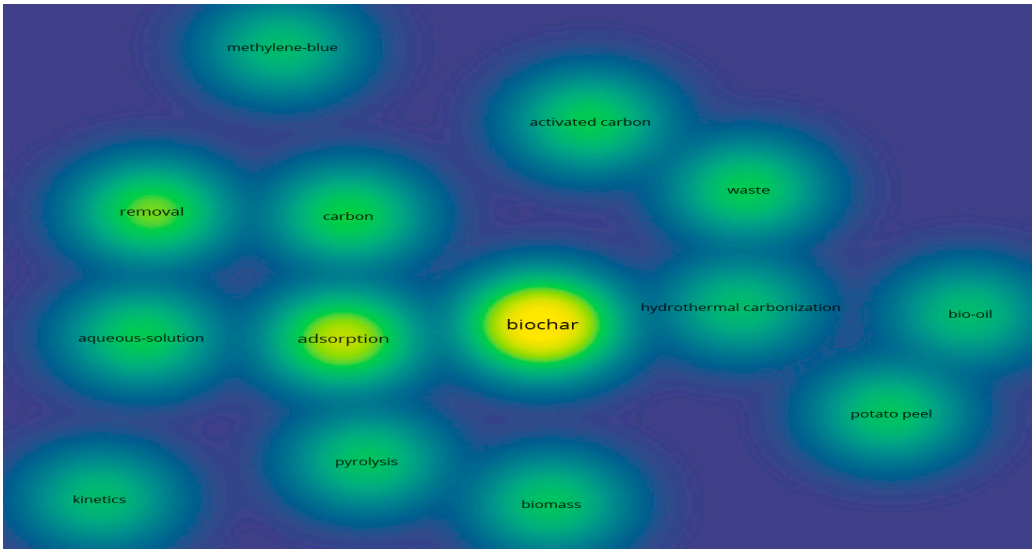

Figure 11. Bibliometric map generated based on density visualization.

Therefore, there is a noticeable gap in the literature regarding biochar derived from specific agro-wastes like apple and potato peels, especially in relation to pollutant removal. In this context, the apple and potato peel biochar obtained at 250 °C and 800 °C were tested for NO_3^- adsorption [87]. The used experimental conditions were the optimal parameters evaluated by our team in previous studies [32,87], where different types of biomass were used to obtain adsorbents. The comparison of the nitrate sorption efficiency of various biochar data are presented in Table 6.

Table 6. The comparison of the nitrate sorption efficiency of various biochar data.

Adsorbent	Experiment Condition	Nitrate Efficiency Removal (%)	References
Magnetic biochar at 550 °C	300 ppm NO_3^-, 0.25 g biochar, 120 min, pH 7,	71.46	[87]
Thermally treated black tea waste at 400 °C	300 ppm NO_3^-, 0.2 g adsorbent, 90 min, pH 6.5,	73.71	[32]
Black tea waste, at 105 °C	300 ppm NO_3^-, 0.2 g adsorbent, 90 min, pH 6.5,	79.25	[32]
Apple peel at 250 °C	300 ppm NO_3^-, 0.2 g adsorbent, 90 min, pH 6.5,	68.54	This study
Apple peel at 800 °C	300 ppm NO_3^-, 0.2 g adsorbent, 90 min, pH 6.5,	52.78	This study
Potato peel at 250 °C	300 ppm NO_3^-, 0.2 g adsorbent, 90 min, pH 6.5,	64.10	This study
Potato peel at 800 °C	300 ppm NO_3^-, 0.2 g adsorbent, 90 min, pH 6.5,	45.46	This study

As can be seen compared with previous studies the apple and potato peel pyrolyzed at 250 °C have lower nitrate efficiency with difference values between 10.71 and 15.15%. The same behavior was observed also for the samples pyrolyzed at 800 °C, which exhibited a nitrate efficiency removal of 52.78% for apple peel and 45.46% for potato peel, respectively. These results can be explained by the fact that the optimal parameters for each individual sample have not been determined, they depend on the physico-chemical characteristics of each sample. According to Gai, et al. [88], the feedstock and temperature during pyrolysis can influence molecular structure and pores size distribution of biochar, and thus affect biochar sorption characteristics. Sohi, et al. [89] reported that different feedstocks developed biochars with varying values of surface area, porosity, and functional groups; factors that have an impact on the sorption properties of the biochars. According to Sun, et al. [90], even though two types of biochar were produced at the same temperature (400 °C), the biochar made from poultry litter had a higher specific surface area and porosity than the biochar made from wheat straw. It should also be mentioned that, in order to reduce the residual washing water, the 4 adsorbents prepared in this study, were tested without being subjected to other treatments, as was conducted for the magnetic adsorbent and black tea waste which were washed with deionized water for several times. There are other studies which indicates that the washing of biochar with water and acid leads to the removal of ash from the pores, thus creating new additional adsorption centers facilitating the retention of the nitrate anion [88,91,92]. Therefore, in the future studies, the optimal parameters for each obtained biochar will be determined and how the washing step influences the efficiency of nitrate retention.

4. Conclusions

This study investigated the impact of pyrolysis temperature on the kinetic parameters, physicochemical characteristics, and structural properties of apple and potato peels to be used as adsorbents. The thermal stability of the biomass waste was evaluated by thermogravimetric analysis. The proximate analysis of apple and potato peel waste indicated high volatile matter content and low ash content of the fixed carbon, suggesting good potential to produce high yields of biochar. The degradation of biomass samples was studied between 25 and 800 °C at different heating rates (5, 10, 20, and 30 °C/min). The results showed that moisture content of the biomass sample is almost 5% of the initial weight. The second stage of degradation corresponding to devolatilization differs slightly due to the composition of the analyzed sample. The potato peel showed one degradation peak in the range 205–375 °C, with 50% weight loss, associated with starch pyrolysis. The

weight loss of around 10% over 355 °C was attributed to the decomposition of cellulose and lignin derivatives present in potato peel. Apple peel devolatilization degradation takes place in two stages: one with a weight loss of 38% and maximum around 220 °C, caused by degradation of simple carbohydrates, and the second peak between 280 and 380 °C with a maximum at 330 °C and a weight loss of approximately 24%, which is attributed to cellulose degradation. The broad peak that starts at a temperature above 375 °C is attributed to lignin degradation that occurs over a wide temperature range. The decomposition kinetics were analyzed using thermal data collected under non-isothermal conditions with a constant heating rate based on both model-free and model-fit approaches. The results showed values of the activation energies in agreement with those from other biomass decomposition studies. The effect of temperature on biomass waste surface structure showed that the surface morphologies of both samples are influenced by the pyrolysis temperature. Pyrolysis of apple and potato peels at 250 °C produced a smooth surface with minimal visible pores; meanwhile, at a temperature of 800 °C, the biochar exhibited deep porous channels with cavity diameters measuring less than 40 µm for the potato peel and less than 30 µm for the apple peel. These observations are also supported by the FTIR analysis, which indicates the disappearance of the bands characteristic of the hydroxyl, aliphatic, ether, and ester functional groups. The elemental analysis also confirms the loss of functional groups due to dehydration and deoxygenation reactions, indicating a carbon percentage of 66.52 and 77.78% for potato and apple peel, respectively. The findings of this study can offer useful insights for biomass waste conversion, namely apple and potato waste can be modeled to obtain adsorbents by adjusting the pyrolysis temperature, which leads to formation of porous structure and, thus, enhances the adsorption capacity. Significant depth to the research is added by using different analytical techniques (FTIR, SEM, EDS) to explore the impact of pyrolysis temperature on the structural characteristics and surface chemistry of biochar.

Author Contributions: Conceptualization: E.-E.S., C.C. and I.B.; formal analysis: D.R.P., M.T. and R.G.; funding acquisition: D.R.P. and E.-E.S.; investigation: C.C. and M.T.; methodology: C.C. and I.B.; supervision: E.-E.S. and M.T.; writing—original draft: E.-E.S., C.C. and I.B.; writing—review and editing: E.-E.S., C.C. and R.G. All authors have read and agreed to the published version of the manuscript.

Funding: The authors thankfully acknowledge the Petroleum-Gas University of Ploiesti, Romania for the financial support, project GO-GICS number 11059/08.06.2023.

Institutional Review Board Statement: Not applicable.

Informed Consent Statement: Not applicable.

Data Availability Statement: The original contributions presented in the study are included in the article, further inquiries can be directed to the corresponding author.

Conflicts of Interest: The authors declare that they have no known competing financial interests or personal relationships that could have appeared to influence the work reported in this paper.

References

1. Wang, X.; Zhou, W.; Liang, G.; Song, D.; Zhang, X. Characteristics of maize biochar with different pyrolysis temperatures and its effects on organic carbon, nitrogen and enzymatic activities after addition to fluvo-aquic soil. *Sci. Total Environ.* **2015**, *538*, 137–144. [CrossRef] [PubMed]
2. Kwapinski, W.; Byrne, C.M.P.; Kryachko, E.; Wolfram, P.; Adley, C.; Leahy, J.J.; Novotny, E.H.; Hayes, M.H.B. Biochar from Biomass and Waste. *Waste Biomass Valorization* **2010**, *1*, 177–189. [CrossRef]
3. Mishra, R.K.; Mohanty, K. A review of the next-generation biochar production from waste biomass for material applications. *Sci. Total Environ.* **2023**, *904*, 167171. [CrossRef]
4. Koçer, A.T.; Erarslan, A.; Özçimen, D. Pyrolysis of Aloe vera leaf wastes for biochar production: Kinetics and thermodynamics analysis. *Ind. Crops Prod.* **2023**, *204*, 117354. [CrossRef]
5. Park, J.-H.; Wang, J.J.; Meng, Y.; Wei, Z.; DeLaune, R.D.; Seo, D.-C. Adsorption/desorption behavior of cationic and anionic dyes by biochars prepared at normal and high pyrolysis temperatures. *Colloids Surf. A Physicochem. Eng. Asp.* **2019**, *572*, 274–282. [CrossRef]

6. Hussin, F.; Aroua, M.K.; Szlachta, M. Biochar derived from fruit by-products using pyrolysis process for the elimination of Pb(II) ion: An updated review. *Chemosphere* **2022**, *287*, 132250. [CrossRef]
7. Maria-Cristina, S.; Gabriela-Dalila, S.; Andreea-Daniela, G.; Andreea- Carmen-Elena, D. An Overview Of Potato Imports From Romania. *Proc. Int. Manag. Conf.* **2022**, *16*, 532–538. [CrossRef]
8. Mushtaq, Q.; Ishtiaq, U.; Joly, N.; Martin, P.; Qazi, J. Investigation and characterization of changes in potato peels by thermochemical acidic pre-treatment for extraction of various compounds. *Sci. Rep.* **2024**, *14*, 12655. [CrossRef]
9. Sampaio, S.L.; Petropoulos, S.A.; Alexopoulos, A.; Heleno, S.A.; Santos-Buelga, C.; Barros, L.; Ferreira, I.C.F.R. Potato peels as sources of functional compounds for the food industry: A review. *Trends Food Sci. Technol.* **2020**, *103*, 118–129. [CrossRef]
10. Gebrechristos, H.Y.; Chen, W. Utilization of potato peel as eco-friendly products: A review. *Food Sci. Nutr.* **2018**, *6*, 1352–1356. [CrossRef]
11. Chohan, N.A.; Aruwajoye, G.S.; Sewsynker-Sukai, Y.; Gueguim Kana, E.B. Valorisation of potato peel wastes for bioethanol production using simultaneous saccharification and fermentation: Process optimization and kinetic assessment. *Renew. Energy* **2020**, *146*, 1031–1040. [CrossRef]
12. Maragkaki, A.E.; Kotrotsios, T.; Samaras, P.; Manou, A.; Lasaridi, K.; Manios, T. Quantitative and Qualitative Analysis of Biomass from Agro-industrial Processes in the Central Macedonia Region, Greece. *Waste Biomass Valorization* **2016**, *7*, 383–395. [CrossRef]
13. Eurostat Database. Available online: https://ec.europa.eu/eurostat/data/database (accessed on 10 August 2022).
14. Vlad, I.M.; Butcaru, A.C.; Fîntîneru, G.; Bădulescu, L.; Stănică, F.; Toma, E. Mapping the Preferences of Apple Consumption in Romania. *Horticulturae* **2023**, *9*, 35. [CrossRef]
15. Rabetafika, H.N.; Bchir, B.; Blecker, C.; Richel, A. Fractionation of apple by-products as source of new ingredients: Current situation and perspectives. *Trends Food Sci. Technol.* **2014**, *40*, 99–114. [CrossRef]
16. Kaur, M.; Kaur, M.; Kaur, H. Apple peel as a source of dietary fiber and antioxidants: Effect on batter rheology and nutritional composition, textural and sensory quality attributes of muffins. *J. Food Meas. Charact.* **2022**, *16*, 2411–2421. [CrossRef]
17. Enniya, I.; Rghioui, L.; Jourani, A. Adsorption of hexavalent chromium in aqueous solution on activated carbon prepared from apple peels. *Sustain. Chem. Pharm.* **2018**, *7*, 9–16. [CrossRef]
18. Urgel, J.J.D.T.; Briones, J.M.A.; Diaz, E.B.; Dimaculangan, K.M.N.; Rangel, K.L.; Lopez, E.C.R. Removal of diesel oil from water using biochar derived from waste banana peels as adsorbent. *Carbon Res.* **2024**, *3*, 13. [CrossRef]
19. Nguyen, V.-T.; Nguyen, T.-B.; Vo, T.-D.-H.; Dat, N.D.; Vo, T.-K.Q.; Nguyen, X.C.; Dinh, V.-C.; Le, T.-N.-C.; Duong, T.-G.-H.; Bui, M.-H.; et al. Preliminary study of doxycycline adsorption from aqueous solution on alkaline modified biochar derived from banana peel. *Environ. Eng. Res.* **2024**, *29*, 230190–230196. [CrossRef]
20. Zhang, W.; Wang, Y.; Fan, L.; Liu, X.; Cao, W.; Ai, H.; Wang, Z.; Liu, X.; Jia, H. Sorbent Properties of Orange Peel-Based Biochar for Different Pollutants in Water. *Processes* **2022**, *10*, 856. [CrossRef]
21. Amin, M.T.; Alazba, A.A.; Shafiq, M. Application of the biochar derived from orange peel for effective biosorption of copper and cadmium in batch studies: Isotherm models and kinetic studies. *Arab. J. Geosci.* **2019**, *12*, 46. [CrossRef]
22. Ullah, R.; Ullah, T.; Khan, N. Removal of Heavy Metals from Industrial Effluents using Burnt Potato Peels as Adsorbent. *J. Appl. Organomet. Chem.* **2023**, *3*, 284–293. [CrossRef]
23. Kyzas, G.Z.; Deliyanni, E.A. Modified activated carbons from potato peels as green environmental-friendly adsorbents for the treatment of pharmaceutical effluents. *Chem. Eng. Res. Des.* **2015**, *97*, 135–144. [CrossRef]
24. Gabhane, J.W.; Bhange, V.P.; Patil, P.D.; Bankar, S.T.; Kumar, S. Recent trends in biochar production methods and its application as a soil health conditioner: A review. *SN Appl. Sci.* **2020**, *2*, 1307. [CrossRef]
25. Cho, S.-K.; Igliński, B.; Kumar, G. Biomass based biochar production approaches and its applications in wastewater treatment, machine learning and microbial sensors. *Bioresour. Technol.* **2024**, *391*, 129904. [CrossRef]
26. Pradhan, S.; Parthasarathy, P.; Mackey, H.R.; Al-Ansari, T.; McKay, G. Food waste biochar: A sustainable solution for agriculture application and soil–water remediation. *Carbon Res.* **2024**, *3*, 41. [CrossRef]
27. Barszcz, W.; Łożyńska, M.; Molenda, J. Impact of pyrolysis process conditions on the structure of biochar obtained from apple waste. *Sci. Rep.* **2024**, *14*, 10501. [CrossRef]
28. Elkhalifa, S.; Parthasarathy, P.; Mackey, H.R.; Al-Ansari, T.; Elhassan, O.; Mansour, S.; McKay, G. Biochar development from thermal TGA studies of individual food waste vegetables and their blended systems. In *Biomass Conversion and Biorefinery*; Springer: Berlin/Heidelberg, Germany, 2022. [CrossRef]
29. Lopes, F.C.R.; Pereira, J.C.; Tannous, K. Thermal decomposition kinetics of guarana seed residue through thermogravimetric analysis under inert and oxidizing atmospheres. *Bioresour. Technol.* **2018**, *270*, 294–302. [CrossRef] [PubMed]
30. Anca-Couce, A.; Tsekos, C.; Retschitzegger, S.; Zimbardi, F.; Funke, A.; Banks, S.; Kraia, T.; Marques, P.; Scharler, R.; de Jong, W.; et al. Biomass pyrolysis TGA assessment with an international round robin. *Fuel* **2020**, *276*, 118002. [CrossRef]
31. Santos, V.O.; Araujo, R.O.; Ribeiro, F.C.P.; Colpani, D.; Lima, V.M.R.; Tenório, J.A.S.; Coleti, J.; Falcão, N.P.S.; Chaar, J.S.; de Souza, L.K.C. Analysis of thermal degradation of peach palm (Bactris gasipaes Kunth) seed using isoconversional models. *React. Kinet. Mech. Catal.* **2022**, *135*, 367–387. [CrossRef]
32. Bondarev, A.; Popovici, D.R.; Călin, C.; Mihai, S.; Sîrbu, E.-E.; Doukeh, R. Black Tea Waste as Green Adsorbent for Nitrate Removal from Aqueous Solutions. *Materials* **2023**, *16*, 4285. [CrossRef]
33. Wang, S.; Dai, G.; Yang, H.; Luo, Z. Lignocellulosic biomass pyrolysis mechanism: A state-of-the-art review. *Prog. Energy Combust. Sci.* **2017**, *62*, 33–86. [CrossRef]

34. Shen, D.; Jin, W.; Hu, J.; Xiao, R.; Luo, K. An overview on fast pyrolysis of the main constituents in lignocellulosic biomass to valued-added chemicals: Structures, pathways and interactions. *Renew. Sustain. Energy Rev.* **2015**, *51*, 761–774. [CrossRef]
35. Vyazovkin, S.; Wight, C.A. Model-free and model-fitting approaches to kinetic analysis of isothermal and nonisothermal data. *Thermochim. Acta* **1999**, *340–341*, 53–68. [CrossRef]
36. Cai, J.; Xu, D.; Dong, Z.; Yu, X.; Yang, Y.; Banks, S.W.; Bridgwater, A.V. Processing thermogravimetric analysis data for isoconversional kinetic analysis of lignocellulosic biomass pyrolysis: Case study of corn stalk. *Renew. Sustain. Energy Rev.* **2018**, *82*, 2705–2715. [CrossRef]
37. Gîjiu, C.L.; Isopescu, R.; Dinculescu, D.; Memecică, M.; Apetroaei, M.R.; Anton, M.; Schröder, V.; Rău, I. Crabs Marine Waste—A Valuable Source of Chitosan: Tuning Chitosan Properties by Chitin Extraction Optimization. *Polymers* **2022**, *14*, 4492. [CrossRef]
38. Dinculescu, D.D.; Apetroaei, M.R.; Gîjiu, C.L.; Anton, M.; Enache, L.; Schröder, V.; Isopescu, R.; Rău, I. Simultaneous Optimization of Deacetylation Degree and Molar Mass of Chitosan from Shrimp Waste. *Polymers* **2024**, *16*, 170. [CrossRef] [PubMed]
39. Silva, J.; Teixeira, S.; Teixeira, J. A Review of Biomass Thermal Analysis, Kinetics and Product Distribution for Combustion Modeling: From the Micro to Macro Perspective. *Energies* **2023**, *16*, 6705. [CrossRef]
40. Phuakpunk, K.; Chalermsinsuwan, B.; Assabumrungrat, S. Pyrolysis kinetic parameters investigation of single and tri-component biomass: Models fitting via comparative model-free methods. *Renew. Energy* **2022**, *182*, 494–507. [CrossRef]
41. Abdelouahed, L.; Leveneur, S.; Vernieres-Hassimi, L.; Balland, L.; Taouk, B. Comparative investigation for the determination of kinetic parameters for biomass pyrolysis by thermogravimetric analysis. *J. Therm. Anal. Calorim.* **2017**, *129*, 1201–1213. [CrossRef]
42. Nourelhouda, B.; Lokmane, A.; Mustapha, C.; Chetna, M.; Abdeslam Hassen, M.; Bechara, T. Investigations on Mediterranean biomass pyrolysis ability by thermogravimetric analyses: Thermal behaviour and sensitivity of kinetic parameters. *Comptes Rendus. Chim.* **2020**, *23*, 623–634. [CrossRef]
43. Meng, H.; Yang, H.; Wu, Z.; Li, D.; Wang, Z.; Wang, D.; Wang, H.; Li, H.; Li, J. Co-Pyrolysis of Mushroom Residue Blended with Pine Sawdust/Wheat Straw for Sustainable Utilization of Biomass Wastes: Thermal Characteristics, Kinetic/Thermodynamic Analysis, and Structure Evolution of Co-Pyrolytic Char. *Sustainability* **2024**, *16*, 6677. [CrossRef]
44. Jemaa, M.; Mohammed Ammar, A.; Besma, K.; Salah, J.; Mejdi, J. Investigations on potential Tunisian biomasses energetic valorization: Thermogravimetric characterization and kinetic degradation analysis. *Comptes Rendus. Chim.* **2022**, *25*, 81–92. [CrossRef]
45. Velciov, A.-B.; Rivis, A.; Popescu, G.-S.; Cozma, A.; Stoin, D.; Anghel, I.-M.; Rada, M.; Hadaruga, N.-G. Preliminary research on the obtaining and nutritional characterization of apple peel powder. *J. Agroaliment. Process. Technol.* **2022**, *28*, 375–380.
46. Reza, M.S.; Ahmed, A.; Caesarendra, W.; Abu Bakar, M.S.; Shams, S.; Saidur, R.; Aslfattahi, N.; Azad, A.K. Acacia Holosericea: An Invasive Species for Bio-char, Bio-oil, and Biogas Production. *Bioengineering* **2019**, *6*, 33. [CrossRef]
47. Ahmed, A.; Bakar, M.S.A.; Razzaq, A.; Hidayat, S.; Jamil, F.; Amin, M.N.; Sukri, R.S.; Shah, N.S.; Park, Y.-K. Characterization and Thermal Behavior Study of Biomass from Invasive Acacia mangium Species in Brunei Preceding Thermochemical Conversion. *Sustainability* **2021**, *13*, 5249. [CrossRef]
48. de Andrade Lima, M.; Andreou, R.; Charalampopoulos, D.; Chatzifragkou, A. Supercritical Carbon Dioxide Extraction of Phenolic Compounds from Potato (Solanum tuberosum) Peels. *Appl. Sci.* **2021**, *11*, 3410. [CrossRef]
49. Müsellim, E.; Tahir, M.H.; Ahmad, M.S.; Ceylan, S. Thermokinetic and TG/DSC-FTIR study of pea waste biomass pyrolysis. *Appl. Therm. Eng.* **2018**, *137*, 54–61. [CrossRef]
50. Zhang, J.; Liu, J.; Evrendilek, F.; Zhang, X.; Buyukada, M. TG-FTIR and Py-GC/MS analyses of pyrolysis behaviors and products of cattle manure in CO_2 and N_2 atmospheres: Kinetic, thermodynamic, and machine-learning models. *Energy Convers. Manag.* **2019**, *195*, 346–359. [CrossRef]
51. da Silva, M.D.; da Boit Martinello, K.; Knani, S.; Lütke, S.F.; Machado, L.M.M.; Manera, C.; Perondi, D.; Godinho, M.; Collazzo, G.C.; Silva, L.F.O.; et al. Pyrolysis of citrus wastes for the simultaneous production of adsorbents for Cu(II), H2, and d-limonene. *Waste Manag.* **2022**, *152*, 17–29. [CrossRef]
52. Ali, S.M.; Siddique, Y.; Mehnaz, S.; Sadiq, M.B. Extraction and characterization of starch from low-grade potatoes and formulation of gluten-free cookies containing modified potato starch. *Heliyon* **2023**, *9*, e19581. [CrossRef]
53. Singh, S.; Wu, C.; Williams, P.T. Pyrolysis of waste materials using TGA-MS and TGA-FTIR as complementary characterisation techniques. *J. Anal. Appl. Pyrolysis* **2012**, *94*, 99–107. [CrossRef]
54. Kouřimská, L.; Kubaschová, K.; Sus, J.; Nový, P.; Dvořáková, B.; Koudela, M. Comparison of the carbohydrate content in apples and carrots grown in organic and integrated farming systems. *Potravin. Slovak J. Food Sci.* **2014**, *8*, 178–183. [CrossRef]
55. Zlatanović, S.; Ostojić, S.; Micić, D.; Rankov, S.; Dodevska, M.; Vukosavljević, P.; Gorjanović, S. Thermal behaviour and degradation kinetics of apple pomace flours. *Thermochim. Acta* **2019**, *673*, 17–25. [CrossRef]
56. Çepelioğullar, Ö.; Haykırı-Açma, H.; Yaman, S. Kinetic modelling of RDF pyrolysis: Model-fitting and model-free approaches. *Waste Manag.* **2016**, *48*, 275–284. [CrossRef]
57. Liu, N.A.; Fan, W.C.; Dobashi, R.; Huang, L.S. Kinetic modeling of thermal decomposition of natural cellulosic materials in air atmosphere. *J. Anal. Appl. Pyrolysis* **2002**, *63*, 303–325. [CrossRef]
58. Emiola-Sadiq, T.; Zhang, L.; Dalai, A.K. Thermal and Kinetic Studies on Biomass Degradation via Thermogravimetric Analysis: A Combination of Model-Fitting and Model-Free Approach. *ACS Omega* **2021**, *6*, 22233–22247. [CrossRef]

59. Li, B.; Ng, J.-H.; Woon, K.S.; Chong, W.W.F.; Ng, K.L.A.; Lee, C.T.; Chiong, M.C.; Nge, K.S.; Mong, G.R. Comparative analysis of kinetic model-fitting methods and selection priority for horse manure pyrolysis. *Sustain. Chem. Pharm.* **2024**, *39*, 101590. [CrossRef]
60. Friedman, H.L. Kinetics of thermal degradation of char-forming plastics from thermogravimetry. Application to a phenolic plastic. *J. Polym. Sci. Part C Polym. Symp.* **1964**, *6*, 183–195. [CrossRef]
61. Ozawa, T. A New Method of Analyzing Thermogravimetric Data. *Bull. Chem. Soc. Jpn.* **1965**, *38*, 1881–1886. [CrossRef]
62. Flynn, J.H.; Wall, L.A. General Treatment of the Thermogravimetry of Polymers. *J. Res. Natl. Bur. Stand. Sect. A Phys. Chem.* **1966**, *70a*, 487–523. [CrossRef]
63. Kissinger, H.E. Variation of Peak Temperature With Heating Rate in Differential Thermal Analysis. *J. Res. Natl. Bur. Stand.* **1956**, *57*, 217. [CrossRef]
64. Starink, M.J. Activation energy determination for linear heating experiments: Deviations due to neglecting the low temperature end of the temperature integral. *J. Mater. Sci.* **2007**, *42*, 483–489. [CrossRef]
65. Vyazovkin, S.; Burnham, A.K.; Criado, J.M.; Pérez-Maqueda, L.A.; Popescu, C.; Sbirrazzuoli, N. ICTAC Kinetics Committee recommendations for performing kinetic computations on thermal analysis data. *Thermochim. Acta* **2011**, *520*, 1–19. [CrossRef]
66. Vyazovkin, S.; Dollimore, D. Linear and Nonlinear Procedures in Isoconversional Computations of the Activation Energy of Nonisothermal Reactions in Solids. *J. Chem. Inf. Comput. Sci.* **1996**, *36*, 42–45. [CrossRef]
67. Balogun, A.O.; Lasode, O.A.; McDonald, A.G. Devolatilisation kinetics and pyrolytic analyses of Tectona grandis (teak). *Bioresour. Technol.* **2014**, *156*, 57–62. [CrossRef]
68. Luangkiattikhun, P.; Tangsathitkulchai, C.; Tangsathitkulchai, M. Non-isothermal thermogravimetric analysis of oil-palm solid wastes. *Bioresour. Technol.* **2008**, *99*, 986–997. [CrossRef]
69. Ko, K.-H.; Rawal, A.; Sahajwalla, V. Analysis of thermal degradation kinetics and carbon structure changes of co-pyrolysis between macadamia nut shell and PET using thermogravimetric analysis and 13C solid state nuclear magnetic resonance. *Energy Convers. Manag.* **2014**, *86*, 154–164. [CrossRef]
70. Pistor, V.; Ornaghi, F.G.; Ornaghi, H.L., Jr.; Zattera, A.J. Degradation kinetic of epoxy nanocomposites containing different percentage of epoxycyclohexyl—POSS. *Polym. Compos.* **2012**, *33*, 1224–1232. [CrossRef]
71. Grioui, N.; Halouani, K.; Zoulalian, A.; Halouani, F. Thermogravimetric analysis and kinetics modeling of isothermal carbonization of olive wood in inert atmosphere. *Thermochim. Acta* **2006**, *440*, 23–30. [CrossRef]
72. Tripathi, M.; Sahu, J.N.; Ganesan, P. Effect of process parameters on production of biochar from biomass waste through pyrolysis: A review. *Renew. Sustain. Energy Rev.* **2016**, *55*, 467–481. [CrossRef]
73. Ottah, V.E.; Ezugwu, A.L.; Ezike, T.C.; Chilaka, F.C. Comparative analysis of alkaline-extracted hemicelluloses from Beech, African rose and Agba woods using FTIR and HPLC. *Heliyon* **2022**, *8*, e09714. [CrossRef] [PubMed]
74. Vassileva, P.; Tumbalev, V.; Kichukova, D.; Voykova, D.; Kovacheva, D.; Spassova, I. Study on the Dye Removal from Aqueous Solutions by Graphene-Based Adsorbents. *Materials* **2023**, *16*, 5754. [CrossRef] [PubMed]
75. Patra, B.R.; Nanda, S.; Dalai, A.K.; Meda, V. Slow pyrolysis of agro-food wastes and physicochemical characterization of biofuel products. *Chemosphere* **2021**, *285*, 131431. [CrossRef] [PubMed]
76. Wystalska, K.; Kwarciak-Kozłowska, A. The Effect of Biodegradable Waste Pyrolysis Temperatures on Selected Biochar Properties. *Materials* **2021**, *14*, 1644. [CrossRef]
77. Park, J.H.; Ok, Y.S.; Kim, S.H.; Kang, S.W.; Cho, J.S.; Heo, J.S.; Delaune, R.D.; Seo, D.C. Characteristics of biochars derived from fruit tree pruning wastes and their effects on lead adsorption. *J. Korean Soc. Appl. Biol. Chem.* **2015**, *58*, 751–760. [CrossRef]
78. Costa, J.M.; Ampese, L.C.; Ziero, H.D.D.; Sganzerla, W.G.; Forster-Carneiro, T. Apple pomace biorefinery: Integrated approaches for the production of bioenergy, biochemicals, and value-added products—An updated review. *J. Environ. Chem. Eng.* **2022**, *10*, 108358. [CrossRef]
79. Guardia, L.; Suárez, L.; Querejeta, N.; Rodríguez Madrera, R.; Suárez, B.; Centeno, T.A. Apple Waste: A Sustainable Source of Carbon Materials and Valuable Compounds. *ACS Sustain. Chem. Eng.* **2019**, *7*, 17335–17343. [CrossRef]
80. Streit, A.F.M.; Collazzo, G.C.; Druzian, S.P.; Verdi, R.S.; Foletto, E.L.; Oliveira, L.F.S.; Dotto, G.L. Adsorption of ibuprofen, ketoprofen, and paracetamol onto activated carbon prepared from effluent treatment plant sludge of the beverage industry. *Chemosphere* **2021**, *262*, 128322. [CrossRef]
81. Rasool, S.; Rasool, T.; Gani, K.M. Understanding the carbendazim adsorption from water using biochar derived from apple pomace and industrial wastewater sludge: Experimental and DFT approaches. *Environ. Sci. Pollut. Res.* **2024**, *31*, 47818–47835. [CrossRef]
82. Yang, H.I.; Lou, K.; Rajapaksha, A.U.; Ok, Y.S.; Anyia, A.O.; Chang, S.X. Adsorption of ammonium in aqueous solutions by pine sawdust and wheat straw biochars. *Environ. Sci. Pollut. Res.* **2018**, *25*, 25638–25647. [CrossRef]
83. Xue, L.; Gao, B.; Wan, Y.; Fang, J.; Wang, S.; Li, Y.; Muñoz-Carpena, R.; Yang, L. High efficiency and selectivity of MgFe-LDH modified wheat-straw biochar in the removal of nitrate from aqueous solutions. *J. Taiwan Inst. Chem. Eng.* **2016**, *63*, 312–317. [CrossRef]
84. Zhang, M.; Song, G.; Gelardi, D.L.; Huang, L.; Khan, E.; Mašek, O.; Parikh, S.J.; Ok, Y.S. Evaluating biochar and its modifications for the removal of ammonium, nitrate, and phosphate in water. *Water Res.* **2020**, *186*, 116303. [CrossRef] [PubMed]

85. Fatima, I.; Ahmad, M.; Vithanage, M.; Iqbal, S. Abstraction of nitrates and phosphates from water by sawdust- and rice husk-derived biochars: Their potential as N- and P-loaded fertilizer for plant productivity in nutrient deficient soil. *J. Anal. Appl. Pyrolysis* **2021**, *155*, 105073. [CrossRef]
86. Clough, T.J.; Condron, L.M.; Kammann, C.; Müller, C. A Review of Biochar and Soil Nitrogen Dynamics. *Agronomy* **2013**, *3*, 275–293. [CrossRef]
87. Oprescu, E.-E.; Enascuta, E.C.; Vasilievici, G.; Banu, N.D.; Banu, I. Preparation of magnetic biochar for nitrate removal from aqueous solutions. *React. Kinet. Mech. Catal.* **2022**, *135*, 2629–2642. [CrossRef]
88. Gai, X.; Wang, H.; Liu, J.; Zhai, L.; Liu, S.; Ren, T.; Liu, H. Effects of Feedstock and Pyrolysis Temperature on Biochar Adsorption of Ammonium and Nitrate. *PLoS ONE* **2014**, *9*, e113888. [CrossRef]
89. Sohi, S.P.; Krull, E.; Lopez-Capel, E.; Bol, R. Chapter 2—A Review of Biochar and Its Use and Function in Soil. In *Advances in Agronomy*; Academic Press: Cambridge, MA, USA, 2010; Volume 105, pp. 47–82.
90. Sun, K.; Ro, K.; Guo, M.; Novak, J.; Mashayekhi, H.; Xing, B. Sorption of bisphenol A, 17α-ethinyl estradiol and phenanthrene on thermally and hydrothermally produced biochars. *Bioresour. Technol.* **2011**, *102*, 5757–5763. [CrossRef]
91. Ji, L.; Wan, Y.; Zheng, S.; Zhu, D. Adsorption of Tetracycline and Sulfamethoxazole on Crop Residue-Derived Ashes: Implication for the Relative Importance of Black Carbon to Soil Sorption. *Environ. Sci. Technol.* **2011**, *45*, 5580–5586. [CrossRef]
92. Afkhami, A.; Madrakian, T.; Karimi, Z. The effect of acid treatment of carbon cloth on the adsorption of nitrite and nitrate ions. *J. Hazard. Mater.* **2007**, *144*, 427–431. [CrossRef]

Disclaimer/Publisher's Note: The statements, opinions and data contained in all publications are solely those of the individual author(s) and contributor(s) and not of MDPI and/or the editor(s). MDPI and/or the editor(s) disclaim responsibility for any injury to people or property resulting from any ideas, methods, instructions or products referred to in the content.